strengths extracted from the ISO spectra of HD163296, we obtain a $[S/Si]_{calc} \cong 0.63$. This ratio is consistent with the cosmochemical (solar) abundance[8] of Si and S (atom ratio 0.52). We conclude from this analysis that the sulphur abundance constraints are broadly consistent with the infrared spectra, although the error bars are large. The implication of this analysis is that most if not all of the sulphur resides in solid grains of FeS.

In the diffuse interstellar medium, sulphur is usually not strongly depleted from the gas phase[21], indicating that little sulphur is incorporated into solid grains in this environment. Either iron sulphides are not produced in significant quantities in stellar outflows, or their lifetime in the interstellar medium is very short owing to rapid destruction. One probable mechanism for their destruction is the reduction of iron sulphide through irradiation, a process that produces Fe metal as a by-product and returns sulphur to the gas phase. A similar mechanism is known to occur in lunar Fe-oxides exposed to the solar wind[22] as well as in GEMS (proposed presolar silicate grains) in cometary IDPs[23]. The situation is very different in cold, dense molecular clouds, where sulphur is highly depleted from the gas phase[1]. In these environments, only trace amounts of sulphur in molecular form or in ice mantles are detected[4]. Therefore, we believe the bulk of the depletion must be accommodated through incorporation of sulphur into solid grains of iron sulphide. The bulk of the iron sulphide is formed either in the collapse phase of the molecular cloud, or in the disk surrounding the young star. Support for this hypothesis comes from observations of iron sulphide grains in IDPs which are intimately associated with carbonaceous material showing H and N isotopic signatures of molecular cloud environments[24,25].

From ISO data, crystalline magnesium-rich silicates (forsterite and enstatite) have been recently discovered in a number of sources. It is probable that iron sulphides are manifest in many ISO spectra as well. Iron sulphides, magnesium-rich crystalline silicates and amorphous silicates are the main components of primitive cometary IDPs. These results thus provide new links between primitive IDPs, comets and presolar materials, and resolves a long-standing dilemma. Iron sulphides have long been recognized as a major component of primitive meteoritic materials, but until now they had escaped detection in astronomical observations of objects similar to the early solar nebula. Isotopic measurements for both iron and sulphur in primitive IDPs may uniquely identify presolar iron sulphide grains. A major implication of this work is that early Earth and other Solar System bodies accreted most of their sulphur in the form of crystalline iron sulphide grains. □

Received 30 November 2001; accepted 5 March 2002.

1. Joseph, C. L., Snow, T. E., Seab, C. G. & Crutcher, R. M. Interstellar abundances in dense, moderately reddened lines of sight. I. Observational evidence for density-dependent depletion. *Astrophys. J.* **309,** 771–782 (1986).
2. Schulze, H., Kissel, J. & Jessberger, E. K. in *Stardust to Planetesimals* (eds Pendleton, T. L. & Tielens, A. G. G. M.) *Astron. Soc. Pacific. Conf. Ser.* **122,** 397–414 (1997).
3. Dai, Z. R. & Bradley, J. P. Iron-nickel sulfides in anhydrous interplanetary dust particles. *Geochim. Cosmochim. Acta* **65,** 3601–3612 (2001).
4. Palumbo, M. E., Geballe, T. R. & Tielens, A. G. G. M. Solid carbonyl sulfide (OCS) in dense molecular clouds. *Astrophys. J.* **479,** 839–844 (1997).
5. Meeus, G. *et al.* ISO spectroscopy of circumstellar dust in 14 Herbig Ae/Be systems: Towards an understanding of dust processing. *Astron. Astrophys.* **365,** 476–490 (2001).
6. Waters, L. B. F. M., Molster, F. J. & Waelkens, C. in *Solid Interstellar Matter: The ISO Revolution* (eds D'Hendecourt, L., Joblin, C & Jones, A.) 219–229 (Springer, Berlin, 1998).
7. Henning, T., Begemann, B., Mutschke, H. & Dorschner, J. Optical properties of oxide dust grains. *Astron. Astrophys. Suppl.* **112,** 143–149 (1995).
8. Anders, E. & Grevesse, N. Abundances of the elements—Meteoritic and solar. *Geochim. Cosmochim. Acta* **53,** 197–214 (1988).
9. Kessler, M. F. *et al.* The Infrared Space Observatory (ISO) mission. *Astron. Astrophys.* **315,** L27–L31 (1996).
10. Bouwman, J., de Koter, A., van den Ancker, M. E. & Waters, L. B. F. M. The composition of the circumstellar dust around the Herbig Ae stars AB Aur and HD 163296. *Astron. Astrophys.* **360,** 213–226 (2000).
11. van den Ancker, M. E. *et al.* ISO Spectroscopy of circumstellar dust in the Herbig Ae systems AB Aur and HD 163296. *Astron. Astrophys.* **357,** 325–329 (2000).
12. Lodders, K. & Fegley, B. in *Asymptotic Giant Branch Stars* (eds LeBertre, T., Lebre, A. & Waelkens, C.) 279–293 (IAU Symposium 191, 1999).
13. Begemann, B. *et al.* A laboratory approach to the interstellar sulfide dust problem. *Astrophys. J.* **423,** L71–L74 (1994).
14. Nuth, J. A. *et al.* Laboratory infrared spectra of predicted condensates in carbon-rich stars. *Astrophys. J.* **290,** L41–L43 (1985).
15. Lennie, A. R. & Vaughan, D. J. Kinetics of the marcasite-pyrite transformation: An infrared spectroscopic study. *Am. Mineral.* **77,** 1166–1177 (1992).
16. Hofmeister, A. M., Rosen, L. J. & Speck, A. K. in *Thermal Emission Spectroscopy and Analysis of Dust, Disks, and Regoliths* (eds Sitko, M. L., Sprague, A. L. & Lynch, D. K.) *Astron. Soc. Pacif. Conf. Ser.* **196,** 291–300 (2000).
17. Malfait, K. *et al.* The spectrum of young star HD 100546 observed with the Infrared Space Observatory. *Astron. Astrophys.* **332,** L25–L28 (1998).
18. Crovisier, J. *et al.* The spectrum of comet Hale-Bopp (C/1995 O1) observed with the Infrared Space Observatory at 2.9 astronomical units from the Sun. *Science* **275,** 1904–1907 (1997).
19. Mutschke, H. *et al.* Steps toward interstellar silicate mineralogy. III. The role of aluminum in circumstellar amorphous silicates. *Astron. Astrophys.* **333,** 188–199 (1998).
20. Draine, B. T. & Lee, H. M. Optical properties of interstellar graphite and silicate grains. *Astrophys. J.* **285,** 89–108 (1984).
21. Savage, B. D. & Sembach, K. R. Interstellar abundances from absorption-line observations with the Hubble Space Telescope. *Annu. Rev. Astron. Astrophys.* **34,** 279–330 (1996).
22. Christoffersen, R., Keller, L. P. & McKay, D. S. Microstructure, chemistry, and origin of grain rims on ilmenite from the lunar soil finest fraction. *Meteorit. Planet. Sci.* **31,** 835–848 (1996).
23. Bradley, J. P. Chemically anomalous preaccretionally irradiated grains in interplanetary dust from comets. *Science* **265,** 925–929 (1994).
24. Keller, L. P., Messenger, S. & Bradley, J. P. Analysis of a deuterium-rich interplanetary dust particle and implications for presolar materials in IDPs. *J. Geophys. Res. A* **105,** 10397–10402 (2000).
25. Keller, L. P., Messenger, S., Miller, M. A. & Thomas, K. L. Nitrogen speciation in a ^{15}N-enriched interplanetary dust particle. *Lunar Planet. Sci.* **28,** 1811–1812 (1997).

Acknowledgements

We thank L. Miller, L. Carr and G. Williams at the National Synchrotron Light Source at Brookhaven National Laboratory for technical assistance. Much of this work was performed while L.P.K. was a Senior Research Scientist at MVA, Inc. F.J.M. acknowledges support from an NWO Talent Grant. L.B.F.M.W., S.H., A.d.K. and J.B. acknowledge financial support from an NWO Pioneer Grant. We thank A. Li and D. Wooden for comments on the manuscript. This work was supported in part by NASA and ESA.

Competing interests statement

The authors declare that they have no competing financial interests.

Correspondence and requests for materials should be addressed to L.P.K. (e-mail: lindsay.p.keller@jsc.nasa.gov).

Formation and propagation of matter-wave soliton trains

Kevin E. Strecker*, Guthrie B. Partridge*, Andrew G. Truscott*† & Randall G. Hulet*

** Department of Physics and Astronomy and Rice Quantum Institute, Rice University, Houston, Texas 77251, USA*

Attraction between the atoms of a Bose–Einstein condensate renders it unstable to collapse, although a condensate with a limited number of atoms[1] can be stabilized[2] by confinement in an atom trap. However, beyond this number the condensate collapses[3–5]. Condensates constrained to one-dimensional motion with attractive interactions are predicted to form stable solitons, in which the attractive forces exactly compensate for wave-packet dispersion[1]. Here we report the formation of bright solitons of ^{7}Li atoms in a quasi-one-dimensional optical trap, by magnetically tuning the interactions in a stable Bose–Einstein condensate from repulsive to attractive. The solitons are set in motion by offsetting the optical potential, and are observed to propagate in the potential for many oscillatory cycles without spreading. We observe a soliton train, containing many solitons; repulsive interactions between neighbouring solitons are inferred from their motion.

† Present address: Research School of Physical Sciences and Engineering, Australian National University, Canberra, ACT 0200, Australia.

Dispersion and diffraction cause localized wave packets to spread as they propagate. Solitons may be formed when a nonlinear interaction produces a self-focusing of the wave packet that compensates for dispersion. Such localized structures have been observed in many physical systems including water waves, plasma waves, sound waves in liquid helium, particle physics, and in optics[6]. A Bose–Einstein condensate can be described by the nonlinear Schrödinger equation, for which the interaction term is cubic in the condensate wavefunction[7]. For attractive interactions, this equation has the same form as the equation for an optical wave propagating in a medium with a cubic, self-focusing (Kerr) nonlinearity and, in this sense, bright matter-wave solitons in one dimension are similar to optical solitons in optical fibres. Dark solitons have been recently studied in condensates with repulsive atomic interactions[8–10], but they are limited in that they can only exist within the condensate itself. Bright solitons, on the other hand, may propagate over much larger distances, and are themselves condensates. A similar experiment to ours has recently been performed by L. Khaykovich *et al.* (personal communication).

The degree of radial confinement necessary to achieve soliton stability has been investigated theoretically[11–14]. Assuming cylindrically symmetric harmonic confinement with axial and radial oscillation frequencies of ω_z and ω_r, respectively, radial excitations are suppressed in the so-called quasi-one-dimensional (quasi-1D) regime, where $\hbar\omega_r$ exceeds the magnitude of the mean-field interaction energy. This requirement is equivalent to a limitation on the condensate occupation number of $N < l_r/|a|$, where $l_r = (\hbar/m\omega_r)^{1/2}$ is the radial scale length, m is the atomic mass and a is the s-wave scattering length characterizing the two-body interactions. The interactions are effectively attractive for $a < 0$ and repulsive for $a > 0$. Achievement of the quasi-1D regime has been recently demonstrated in the case of ^{7}Li (ref. 15) and ^{23}Na (ref. 16) condensates.

The apparatus for producing a quantum degenerate gas of ^{7}Li atoms was described previously[17], although a new magnetic trap with axial and radial frequencies of 70 Hz and 800 Hz, respectively, has been incorporated. Atoms in the $(F, m_F) = (2, 2)$ sublevel, where F and m_F are, respectively, the total electronic angular momentum and its projection, are evaporatively cooled in the magnetic trap to a temperature of $\sim$1 μK. Atoms in the (1, 1) state, which are not magnetically trappable, are needed in the final stages of the experiment, so the (2, 2) atoms are transferred to an optical trap. The optical trap consists of a single, focused, red-detuned laser beam propagating in the axial direction for radial confinement, and a separated pair of cylindrically focused blue-detuned laser beams ('end caps') propagating in the radial plane, for axial confinement. The single beam is provided by an infrared Nd:YAG laser, with a wavelength of 1,064 nm, focused to a $1/e^2$ intensity radius of 47 μm and with a power of up to 750 mW. The radial confinement potential is approximately harmonic, and at the highest power, matches well with the magnetic trap potential. This single axial beam provides a very weak axial restoring potential, which is also approximately harmonic, with a frequency of $\sim$4 Hz for oscillation amplitudes less than the Rayleigh length of 6.5 mm. The end caps are generated from the second harmonic of another Nd:YAG laser, have $1/e^2$ radii of 22 μm axially and 100 μm radially, a power of 350 mW in each beam, and are separated by 230 μm. The end caps create a box-like potential in the axial direction, which helps to better match the magnetic trap potential. Once the optical trap lasers are switched on, the magnetic trap is switched off. After 50 ms, a bias field of up to 1,000 G is applied. A period of $\sim$200 ms is allowed for the bias field to stabilize at the chosen value before the atoms are transferred from the (2, 2) state to the (1, 1) state by an adiabatic microwave sweep of 15 ms in duration and 1 MHz in width. The purity of the (1, 1) state population is measured to be greater than 98%.

Attractive interactions between atoms in the (2, 2) state limit the number of possible condensate atoms to a very small fraction of the total number. However, interactions between (1, 1) state atoms at zero magnetic field are repulsive with a scattering length $a = 5a_o$, where a_o is the Bohr radius[18]. Although this fact ensures the stability of the condensate, the rate of its formation is limited by the rate of thermalization, which scales as a^2. In order to increase this rate, a magnetically tuned Feshbach resonance[19,20] is used to increase the magnitude of a. Figure 1 shows the results of a calculation of a versus the magnetic field B, which exhibits a collisional resonance near 725 G. The rate of loss of atoms is observed to increase rapidly near the resonance (Fig. 2), in accordance with previous investigations[20,21]. Atoms are evaporatively cooled in the optical trap by halving the intensity of the infrared beam, and by tuning the bias field to 710 G, where the scattering length is large ($\sim 200a_o$) and positive. Absorption imaging indicates that a condensate is formed with up to $\sim 3 \times 10^5$ atoms. Our techniques are similar to those used to make condensates of ^{85}Rb, where a Feshbach resonance was used to manipulate the sign and magnitude of a (ref. 21).

Following the formation of the condensate at large positive a, the field is ramped down as $e^{-t/\tau}$ (where t is time and $\tau = 40$ ms), to a selected field between 545 G and 630 G, where a is small and negative or small and positive (Fig. 1). The condensate can be created on the side of the optical potential by axially displacing the focus of the infrared beam relative to the centres of the magnetic trap and the box potential formed by the end caps. The end caps

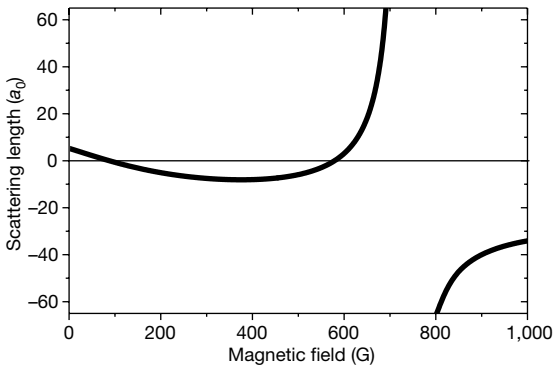

Figure 1 Feshbach resonance. Calculation of the scattering length versus magnetic field for atoms in the (1, 1) state of ^{7}Li using the coupled channels method[18]. The field axis has been scaled here by a factor of 0.91, to agree with the measured resonance position of 725 G shown in Fig. 2. The scattering length is given in units of the Bohr radius, a_o.

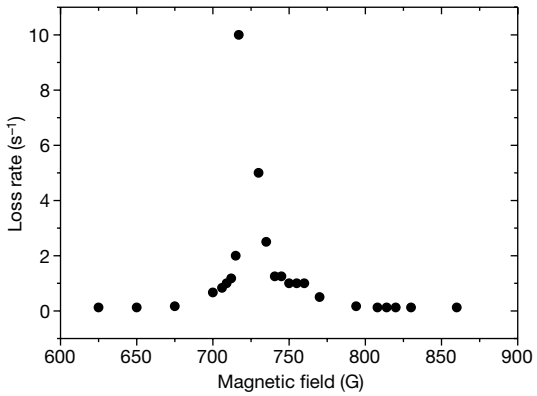

Figure 2 Measured rate of inelastic collisional loss of atoms near the Feshbach resonance. The temperature is $\sim$1 μK, which is above the transition temperature for Bose–Einstein condensation. The initial peak density is estimated to be $\sim 6 \times 10^{12}$ cm^{-3}. The rate of loss is given by the time for the number of trapped atoms to fall to e^{-1} of the initial number. The magnetic field is determined spectroscopically by measuring the frequency of the (2, 2) → (1, 1) transition to within an uncertainty of 0.1 G.

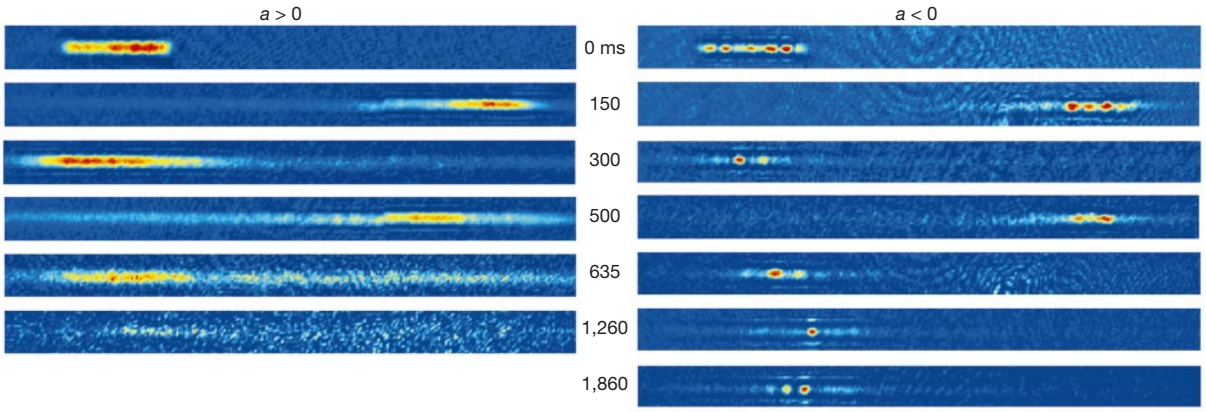

Figure 3 Comparison of the propagation of repulsive condensates with atomic solitons. The images are obtained using destructive absorption imaging, with a probe laser detuned 27 MHz from resonance. The magnetic field is reduced to the desired value before switching off the end caps (see text). The times given are the intervals between turning off the end caps and probing (the end caps are on for the $t = 0$ images). The axial dimension of each image frame corresponds to 1.28 mm at the plane of the atoms. The amplitude of oscillation is ~370 μm and the period is 310 ms. The $a > 0$ data correspond to 630 G, for which $a \approx 10a_0$, and the initial condensate number is $\sim 3 \times 10^5$. The $a < 0$ data correspond to 547 G, for which $a \approx -3a_0$. The largest soliton signals correspond to ~5,000 atoms per soliton, although significant image distortion limits the precision of number measurement. The spatial resolution of ~10 μm is significantly greater than the expected transverse dimension $l_r \approx 1.5$ μm.

prevent the condensate from moving under the influence of the infrared potential until, at a certain instant, the end caps are switched off and the condensate is set in motion. The condensate is allowed to evolve for a set period of time before an image is taken. As shown in Fig. 3, the condensate spreads for $a > 0$, while for $a < 0$, non-spreading, localized structures (solitons) are formed. Solitons have been observed for times exceeding 3 s, a limitation that we believe is due to loss of atoms rather than wave-packet spreading.

Multiple solitons ('soliton trains') are usually observed, as is evident in Figs 3 and 4. We find that typically four solitons are created from an initially stationary condensate. Although multi-soliton states with alternating phase are known to be stationary states of the nonlinear Schrödinger equation[14,22,23], mechanisms for their formation are diverse. It was proposed that a soliton train could be generated by a modulational instability[24], where in the case of a condensate, phase fluctuations would produce a maximum rate of amplitude growth at a wavelength approximately equal to the condensate healing length $\xi = (8\pi n|a|)^{-1/2}$, where n is the atomic density[23]. As a and ξ are dynamically changing in the experiment, the expected number of solitons N_s is not readily estimated from a static model. Experimentally, we detect no significant difference in N_s when the time constant, τ, for changing the magnetic field is varied from 25 ms to 200 ms. We investigated the dependence of N_s on condensate velocity v by varying the interval Δt between the time the end caps are switched off to the time when a changes sign. We find that N_s increases linearly with Δt, from ~4 at $\Delta t = 0$ to ~10 at $\Delta t = 35$ ms. As the axial oscillation period is ~310 ms, $v \propto \Delta t$ in the range of Δt investigated.

The alternating phase structure of the soliton train can be inferred from the relative motion of the solitons. Non-interacting solitons, simultaneously released from different points in a harmonic potential, would be expected to pass through one another. But this is not observed, as can be seen from Fig. 4, which shows that the spacing between the solitons increases near the centre of oscillation and bunches at the end points. This is evidence of a short-range repulsive force between the solitons. Interaction forces between solitons have been found to vary exponentially with the distance between them, and to be attractive or repulsive depending on their relative phase[25]. Because of the effect of wave interference on the kinetic energy, solitons that differ in phase by π will repel, while those that have the same phase will attract. An alternating phase structure can be generated in the initial condensate by a phase

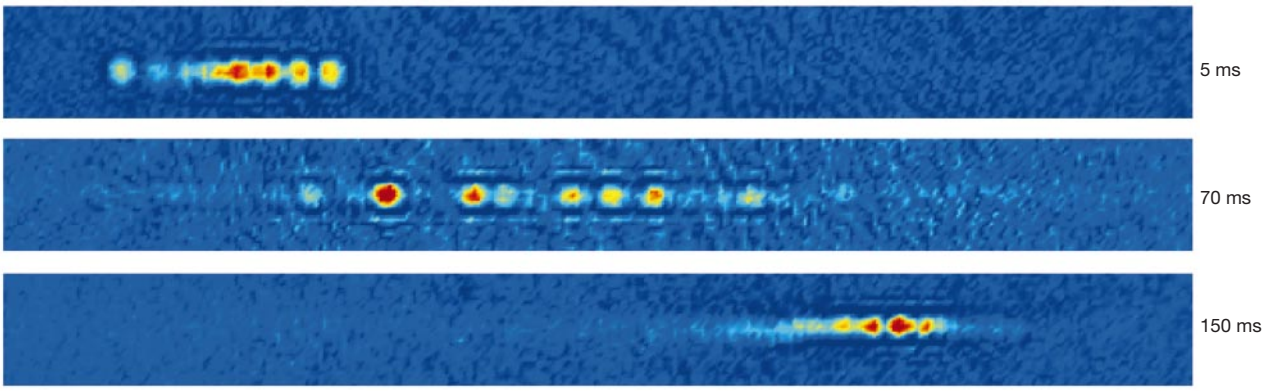

Figure 4 Repulsive interactions between solitons. The three images show a soliton train near the two turning points and near the centre of oscillation. The spacing between solitons is compressed at the turning points, and spread out at the centre of the oscillation. A simple model based on strong, short-range, repulsive forces between nearest-neighbour solitons indicates that the separation between solitons oscillates at approximately twice the trap frequency, in agreement with observations. The number of solitons varies from image to image because of shot to shot experimental variations, and because of a very slow loss of soliton signal with time. As the axial length of a soliton is expected to vary as $1/N$ (ref. 11), solitons with small numbers of atoms produce particularly weak absorption signals, scaling as N^2. Trains with missing solitons are frequently observed, but it is not clear whether this is because of a slow loss of atoms, or because of sudden loss of an individual soliton.

gradient, $d\phi/dz$, across the condensate. Such a gradient may be imprinted by a condensate velocity, because $d\phi/dz = mv/\hbar$, where m is the atomic mass. If N_s is identified with ϕ/π, the model predicts $N_s \propto v$, in agreement with the observed v-dependent part of N_s. Furthermore, for the largest v and for parameters consistent with the experiment, the model gives $N_s \approx 15$, in rough agreement with observation.

For a soliton with $a = -3a_o$, the calculated maximum number of atoms that ensures stability is only ~6,000 per soliton[11,13], which accounts for far fewer atoms than the number contained in the initial repulsive condensate. Apparently, most of the atoms from the collapsing condensate are lost, while only a small fraction remain as solitons. Immediately after switching a from positive to negative, we observe a diffuse background of atoms spreading out axially. This observation is reminiscent of the jet emitted by a ^{85}Rb condensate after switching from repulsive to attractive interactions[5]. In our system, which is in the quasi-1D regime, the remnant atoms form solitons with atom number near their stability limit.

The remarkable similarities between bright matter-wave solitons and optical solitons in fibres[26] emphasize the intimate connection between atom optics with Bose–Einstein condensates[27] and light optics. Many issues remain to be addressed, however, including the dynamical process of soliton formation. In addition, further investigation of soliton interactions and collisions could be undertaken with this system. Finally, we speculate that an 'atomic soliton laser', based on bright matter-wave solitons, may prove useful for precision measurement applications, such as atom interferometry[28]. □

Received 19 March; accepted 18 April 2002.
Published online 1 May 2002, DOI 10.1038/nature747.

1. Ruprecht, P. A., Holland, M. J., Burnett, K. & Edwards, M. Time-dependent solution of the nonlinear Schrodinger equation for Bose-condensed trapped neutral atoms. *Phys. Rev. A* **51,** 4704–4711 (1995).
2. Bradley, C. C., Sackett, C. A. & Hulet, R. G. Bose-Einstein condensation of lithium: observation of limited condensate number. *Phys. Rev. Lett.* **78,** 985–989 (1997).
3. Sackett, C. A., Gerton, J. M., Welling, M. & Hulet, R. G. Measurements of collective collapse in a Bose-Einstein condensate with attractive interactions. *Phys. Rev. Lett.* **82,** 876–879 (1999).
4. Gerton, J. M., Strekalov, D., Prodan, I. & Hulet, R. G. Direct observation of growth and collapse of a Bose–Einstein condensate with attractive interactions. *Nature* **408,** 692–695 (2000).
5. Donley, E. A. *et al.* Dynamics of collapsing and exploding Bose–Einstein condensates. *Nature* **412,** 295–299 (2001).
6. Stegeman, G. I. & Segev, M. Optical spatial solitons and their interactions: Universality and diversity. *Science* **286,** 1518–1523 (1999).
7. Dalfovo, F., Giorgini, S., Pitaevskii, L. P. & Stringari, S. Theory of Bose-Einstein condensation in trapped gases. *Rev. Mod. Phys.* **71,** 463–512 (1999).
8. Burger, S., Bongs, K., Dettmer, S., Ertmer, W. & Sengstock, K. Dark solitons in Bose-Einstein condensates. *Phys. Rev. Lett.* **83,** 5198–5201 (1999).
9. Denschlag, J. *et al.* Generating solitons by phase engineering of a Bose-Einstein condensate. *Science* **287,** 97–100 (2000).
10. Anderson, B. P. *et al.* Watching dark solitons decay into vortex rings in a Bose-Einstein condensate. *Phys. Rev. Lett.* **86,** 2926–2929 (2001).
11. Pérez-García, V., Michinel, H. & Herrero, H. Bose-Einstein solitons in highly asymmetric traps. *Phys. Rev. A* **57,** 3837–3842 (1998).
12. Muryshev, A. E., van Linden van den Heuvell, H. B. & Shlyapnikov, G. V. Stability of standing matter waves in a trap. *Phys. Rev. A* **60,** R2665–R2668 (1999).
13. Carr, L. D., Leung, M. A. & Reinhardt, W. P. Dynamics of the Bose-Einstein condensate: quasi-one-dimension and beyond. *J. Phys. B* **33,** 3983–4001 (2000).
14. Kivshar, Y. S., Alexander, T. J. & Turitsyn, S. K. Nonlinear modes of a macroscopic quantum oscillator. *Phys. Lett. A* **278,** 225–230 (2001).
15. Schreck, F. *et al.* Quasipure Bose-Einstein condensate immersed in a Fermi sea. *Phys. Rev. Lett.* **87,** 080403-1–080403-4 (2001).
16. Görlitz, A. *et al.* Realization of Bose-Einstein condensates in lower dimensions. *Phys. Rev. Lett.* **87,** 130402-1–130402-4 (2001).
17. Truscott, A. G., Strecker, K. E., McAlexander, W. I., Partridge, G. B. & Hulet, R. G. Observation of Fermi pressure in a gas of trapped atoms. *Science* **291,** 2570–2572 (2001).
18. McAlexander, W. I. Collisional Interactions in an Ultracold Lithium Gas. Thesis, Rice Univ. (2000).
19. Tiesinga, E., Verhaar, B. J. & Stoof, H. T. C. Threshold and resonance phenomena in ultracold ground-state collisions. *Phys. Rev. A* **47,** 4114–4122 (1993).
20. Inouye, S. *et al.* Observation of Feshbach resonances in a Bose–Einstein condensate. *Nature* **392,** 151–154 (1998).
21. Roberts, J. L., Claussen, N. R., Cornish, S. L. & Wieman, C. E. Magnetic field dependence of ultracold collisions near a Feshbach resonance. *Phys. Rev. Lett.* **85,** 728–731 (2000).
22. Zakharov, V. E. & Shabat, A. B. Exact theory of two-dimensional self-focusing and one-dimensional self-modulation of waves in nonlinear media. *Sov. Phys. JETP* **34,** 62–65 (1972).
23. Carr, L. D., Clark, C. W. & Reinhardt, W. P. Stationary solutions of the one-dimensional nonlinear Schrödinger equation. II. Case of attractive nonlinearity. *Phys. Rev. A* **62,** 063611-1–063611-10 (2000).
24. Tai, K., Hasegawa, A. & Tomita, A. Observation of modulational instability in optical fibers. *Phys. Rev. Lett.* **56,** 135–138 (1986).
25. Gordon, J. P. Interaction forces among solitons in optical fibers. *Opt. Lett.* **8,** 596–598 (1983).
26. Hasegawa, A. *Optical Solitons in Fibers* (Springer, New York, 1990).
27. Lenz, G., Meystre, P. & Wright, E. M. Nonlinear atom optics. *Phys. Rev. Lett.* **71,** 3271–3274 (1993).
28. Kasevich, M. A. Atom interferometry with Bose-Einstein condensed atoms. *C.R. Acad. Sci. IV* **2,** 497–507 (2001).

Acknowledgements

We thank W. I. McAlexander for providing the coupled channels calculation, B. Luey for making the magnetic coils, and T. Killian and H. Stoof for discussions. This work was supported by the US National Science Foundation, NASA, the Office of Naval Research and the Welch Foundation.

Competing interests statement

The authors declare that they have no competing financial interests.

Correspondence and requests for materials should be addressed to R.G.H. (e-mail: randy@atomcool.rice.edu).

Spin-galvanic effect

S. D. Ganichev*†, E. L. Ivchenko†, V. V. Bel'kov†, S. A. Tarasenko†, M. Sollinger*, D. Weiss*, W. Wegscheider*‡ & W. Prettl*

** Fakultät für Physik, Universität Regensburg, D-93040 Regensburg, Germany*
† A.F. Ioffe Physico-Technical Institute of the RAS, 194021 St Petersburg, Russia
‡ Walter Schottky Institut, TU München, 85748 Garching, Germany

There is much recent interest in exploiting the spin of conduction electrons in semiconductor heterostructures together with their charge to realize new device concepts[1]. Electrical currents are usually generated by electric or magnetic fields, or by gradients of, for example, carrier concentration or temperature. The electron spin in a spin-polarized electron gas can, in principle, also drive an electrical current, even at room temperature, if some general symmetry requirements are met. Here we demonstrate such a 'spin-galvanic' effect in semiconductor heterostructures, induced by a non-equilibrium, but uniform population of electron spins. The microscopic origin for this effect is that the two electronic sub-bands for spin-up and spin-down electrons are shifted in momentum space and, although the electron distribution in each sub-band is symmetric, there is an inherent asymmetry in the spin-flip scattering events between the two sub-bands. The resulting current flow has been detected by applying a magnetic field to rotate an optically oriented non-equilibrium spin polarization in the direction of the sample plane. In contrast to previous experiments, where spin-polarized currents were driven by electric fields in semiconductor[2,3], we have here the complementary situation where electron spins drive a current without the need of an external electric field.

Although it is usually ignored, it is well known that the spin degeneracy of sub-bands in semiconductor quantum well (QW) structures can be lifted, owing to terms linear in the wavevector **k** resulting from the spin orbit interaction in asymmetric potentials[4,5]. For a two-dimensional electron gas (2DEG) system, this leads to the situation sketched in Fig. 1. The electron energy band splits into two sub-bands which are shifted in **k**-space and each of the bands comprise states with spin up or down. In this band structure spin polarization means that one sub-band is occupied up to higher energies than the other. This is depicted in Fig. 1, illustrating that there are more spin-down than spin-up electrons. Can such a situation of uniform spin polarization cause an electric current? As long as the carrier distribution in each sub-band is symmetric around the sub-band minimum at $k_{x_\pm}$ no current flows. However, asymmetric **k**-dependent spin relaxation events can occur, indicated